Article ID: 1000-324X(2020)05-0617-06 **DOI:** 10.15541/jim20190225

La^{3+}-substituted $Sr_2Fe_{1.5}Ni_{0.1}Mo_{0.4}O_{6-\delta}$ as Anodes for Solid Oxide Fuel Cells

XIA Tian[1,2], MENG Xie[1], LUO Ting[1], ZHAN Zhongliang[1]

(1. CAS Key Laboratory of Materials for Energy Conversion, Shanghai Institute of Ceramics, Chinese Academy of Sciences, Shanghai 200050, China; 2. University of Chinese Academy of Sciences, Beijing 100049, China)

Abstract: Lanthanum-substituted $La_xSr_{2-3x/2}Fe_{1.5}Ni_{0.1}Mo_{0.4}O_{6-\delta}$ (La_xSFNM, x=0, 0.1, 0.2, 0.3, 0.4) oxides were synthesized by the solid-state reaction method, and investigated as potential anodes for Solid Oxide Fuel Cells(SOFC). X-ray diffraction patterns of as-synthesized powders confirm the formation of the cubic perovskite structure. Reduction in H_2 promotes the segregation of nano-scale metallic Fe-Ni alloy particles on the grain surfaces. Scanning electron microscopy observations indicate that increasing La^{3+} dopants results in a decrease in the density of the exsolved nanoparticulates. Based upon impedance measurements on symmetrical fuel cells, the anode polarization resistance decreases with the La^{3+} dopant increasing, and attains a minimal value of 0.16 $\Omega\cdot cm^2$ for $La_{0.3}$SFNM at 750 ℃, followed by a slight increase to 0.17 $\Omega\cdot cm^2$ for $La_{0.4}$SFNM. The highest catalytic activity of $La_{0.3}$SFNM toward electro-oxidation of hydrogen fuels could be ascribed to the synergy between the exsolved Fe-Ni alloy nanoparticulates and the supporting La_xSFNM oxides. Thin $La_{0.9}Sr_{0.1}Ga_{0.8}Mg_{0.2}O_3$ (LSGM) electrolyte fuel cells with $La_{0.3}$SFNM anodes and $SmBa_{0.5}Sr_{0.5}Co_2O_6$ cathodes exhibit the highest power densities, *e.g.*, 1.26, 0.90 and 0.52 $W\cdot cm^{-2}$ at 750, 650 and 550 ℃, respectively. These results demonstrate $La_{0.3}$SFNM oxide as a promising high performance SOFC anode.

Key words: Solid Oxide Fuel Cells; anode materials; *in-situ* exsolution

With increasing concerns on energy shortage and environment pollution over the last few decades, Solid Oxide Fuel Cells (SOFCs) have gained worldwide attention as a new means of power generation due to their coherent characteristics of high electrical efficiencies and low emissions. As the state-of-the-art anode materials, Ni/YSZ cermets exhibit excellent catalytic activity toward hydrogen oxidation reactions, but very poor redox stability with high susceptibility toward Ni coarsening during the long-term operation[1]. In order to overcome these issues, a series of conductive oxides were investigated as alternative anodes. Some perovskite oxides such as $La_{1-3x/2}Sr_xTiO_{3-\delta}$[2], $La_{0.75}Sr_{0.25}Cr_{0.5}Mn_{0.5}O_{3-\delta}$[3] and $Sr_2Fe_{1.5}Mo_{0.5}O_{6-\delta}$[4] showed promising anode performance owing to their high thermal and chemical stability as well as high mixed ionic and electronic conductivities. Optimization of the chemical composition and the structural defects may allow for some improvements in the anode performance[5–7], nevertheless, their catalytic activity was still much lower than the typical Ni-cermet anodes. Adding a secondary catalyst to the perovskite oxide by infiltration[8-9] or vapor deposition[10] was effective in improving the overall anode performance. It remains a challenge to precisely control their surface morphology with enhanced long-term stability at elevated temperatures.

In-situ exsolution was demonstrated as an elegant and effective approach to obtain nano-scale metal catalysts on the surface of perovskite oxides[11–14]. Specifically, transitional metals such as Ni, Co and Pt were selected to partially substitute the B-sites of the perovskite oxides during the powder synthesis in air, which were then *in-situ* segregated from the lattice and precipitated as metal nanoparticulates in the reducing environments at high temperatures. With an ideal catalyst morphology, these exsolved metal nanoparticulates evenly distributed on the surface of the perovskite oxides. Note that the amounts and sizes of these metal nanoparticulates may significantly affect the anode performance[15]. Moreover, their physical distribution may also change due to the continuous precipitation in the reducing environments at high temperatures[16]. Therefore, it becomes crucial to control the ion segregation kinetics so as to optimize the dimension and density of the exsolved nanoparticulates, thereby

Received date: 2019-05-15; **Revised date:** 2019-05-29
Foundation item: National Natural Science Foundation of China (51672298, 51702344, 51737011); The State of Grid (SGSDJN00FZQT1700446)
Biography: XIA Tian (1993–), male, Master candidate. E-mail: xiatian@student.mail.sic.ac.cn
夏 天(1993–), 男, 硕士研究生. E-mail: xiatian@student.mail.sic.ac.cn
Corresponding author: ZHAN Zhongliang, professor. E-mail: zzhan@mail.sic.ac.cn
占忠亮, 研究员. E-mail: zzhan@mail.sic.ac.cn

enhancing their performance as the anode catalysts[17].

Recently, non-stoichiometry[12] and additional electric field[18] were used to tailor the metal segregation process. Furthermore, the segregation driving force was analyzed by the distribution of relaxation time (DRT) calculations[11,19-20], indicating that ion size mismatch and electrostatic interaction played important roles in the segregation process. Altering the dopant valence and the ion size may change the exsolution behaviour. In this work, lanthanum was introduced into the A-site to partially replace Sr^{2+} in $Sr_2Fe_{1.5}Ni_{0.1}Mo_{0.4}O_{6-\delta}$. A series of samples, $La_xSr_{2-3x/2}Fe_{1.5}Ni_{0.1}Mo_{0.4}O_{6-\delta}$ (x=0–0.4), were synthesized in air. The chemical compositions were examined before and after reduction in H_2 by X-ray diffraction(XRD), with the surface morphology observed using scanning electron microscope (SEM). It was found that La doping could inhibit *in-situ* exsolution of Fe-Ni alloys and improve the stability of ceramic substrates. Symmetrical anode fuel cells and functioning fuel cells were fabricated by the impregnation method and tested to verify optimization of the anode performance for $La_xSr_{2-3x/2}Fe_{1.5}Ni_{0.1}Mo_{0.4}O_{6-\delta}$ at x= 0.3.

1 Experimental

La_xSFNM ($La_xSr_{2-3x/2}Fe_{1.5}Mo_{0.4}Ni_{0.1}O_{6-\delta}$, x=0, 0.1, 0.2, 0.3, 0.4) powders used in this study were synthesized by the standard solid-state reaction method. The starting materials were La_2O_3(>99%), $SrCO_3$ (>98%), Fe_2O_3 (>98%), MoO_3 (>99%) and NiO (>99%). La_2O_3 was fired at 800 ℃ for 12 h before being weighed, and $SrCO_3$ was dried at 150 ℃ to remove the adsorbed water in air. Similar to the synthesis of $Sr_2Fe_{1.5}Mo_{0.5}O_6$(SFM) powders[21], the first step was to prepare $Fe_2Mo_3O_{12}$. Fe_2O_3 and MoO_3 oxides were mixed and thoroughly ground by ball milling in anhydrous ethanol at a stoichiometric ratio of 1:3 with 6wt% triethanolamine as the dispersant. The mixture was heat-treated at 750 ℃ for 12 h with the resulting phase pure $Fe_2Mo_3O_{12}$ oxide confirmed by XRD. Next, a stoichiometric ratio of La_2O_3, $SrCO_3$, Fe_2O_3, $Fe_2Mo_3O_{12}$ and NiO were similarly mixed and ball milled for 12 h in anhydrous ethanol. In order to ensure full decomposition of $SrCO_3$ to SrO and CO_2, the mixture was heated at 3 ℃/min up to 1000 ℃ and held at this temperature for 12 h. After cooling to room temperature, the powders were reground in the mortar, followed by the second heat-treatment at 1200 ℃ for 12 h.

The crystalline structure of as-synthesized La_xSFNM powders was examined by XRD using Rigaku Ultima IV with monochromatic Cu Kα radiation. In order to analyze the ceramic surface morphology after *in-situ* dissolution of metal particles in the reducing environments, ceramic pellets were prepared by uniaxially dry-pressing La_xSFNM powders under 15 MPa, followed by sintering at 1400 ℃ for 5 h in air and reducing at 750 ℃ for 4 h in wet 10vol% H_2/N_2 (3vol% H_2O). SFNM and $La_{0.3}$SFNM samples were further reduced at 800 ℃ in pure hydrogen for 24 h. The surface topography was observed by SEM (Hitachi SU8220 and FEI Inspect F50), and the chemical compositions of the precipitated particles were analyzed by EDS.

Symmetrical anode fuel cells were prepared by the impregnation method, and $La_{0.9}Sr_{0.1}Ga_{0.8}Mg_{0.2}O_3$ (LSGM) was selected as the electrolyte due to its high oxide ionic conductivity. “Porous|dense|porous” LSGM scaffolds were obtained by laminating the tape-casted ceramic green tapes with rice starch as the fugitive material for the porous layers, as reported in our previous publication[22]. The La_xSFNM anode catalysts were added by infiltrating an aqueous solution, containing $La(NO_3)_3$, $Sr(NO_3)_2$, $Fe(NO_3)_3\cdot 9H_2O$, $Ni(NO_3)_2$, $(NH_4)_6Mo_7O_{24}\cdot 4H_2O$ and citric acid at an appropriate ratio, followed by calcinations at 850 ℃ for 30 min. Such a process was repeated until a catalyst loading of 30wt% was achieved after calcination at 1000 ℃ for 4 h to produce the perovskite oxides. The impedance data were measured on the symmetrical anode fuel cells in 97vol% H_2-3vol% H_2O at 100 sccm using the Electrochemical Workstation (ZAHNER IM6e, Germany) over the frequency range of 0.05 Hz to 100 kHz.

To fabricate the functioning fuel cells, $SmBa_{0.5}Sr_{0.5}Co_2O_{5+\delta}$ (SBSCO) was infiltrated as the cathode catalyst into the porous LSGM of the tri-layered scaffolds on one side, with the La_xSFNM anode catalysts infiltrated on the other side. SBSCO was selected as the cathode catalyst owing to its high electrical conductivity and excellent catalytic activity toward oxygen reduction reactions. The effective area of as-prepared fuel cells was 1.05 cm^2. Silver paste (DAD-87, Shanghai Research Institute of Synthetic Resins) was printed on the electrode surface to collect the electrical current. Single cells were sealed on the alumina tubes using the ceramic glue. The anode was reduced in humidified H_2 for 5 h before any electrochemical measurement.

2 Results and discussion

The crystalline structure of as-synthesized powders was determined by room temperature XRD. Fig. 1(a) summarizes the XRD patterns of a series of La_xSFNM (x=0, 0.1, 0.2 0.3 and 0.4) oxides, which can be well

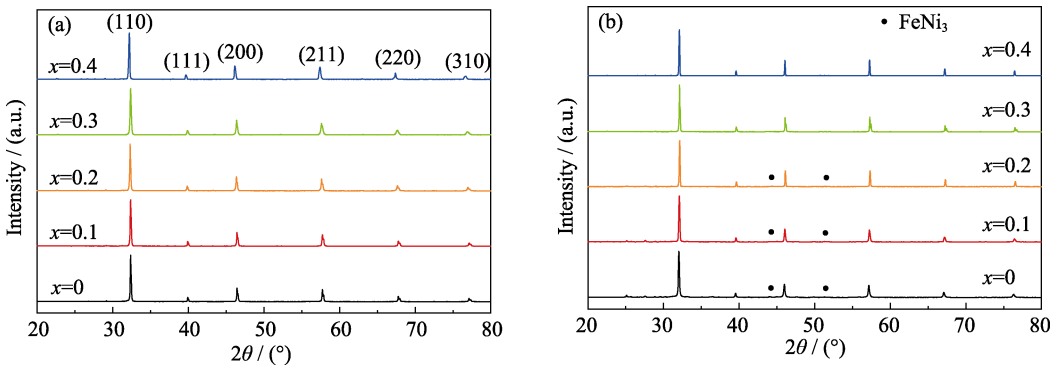

Fig. 1　Room temperature XRD patterns of La_xSFNM (x=0, 0.1, 0.2, 0.3, 0.4)
(a) After calcination at 1200 ℃ for 12 h; (b) Reduced in wet H_2 (3vol% H_2O) at 750 ℃ for 12 h

indexed in single perovskite structure with cubic symmetry. Fig. 1(b) shows the XRD patterns of the thermally treated oxides in wet H_2 (3vol% H_2O) at 750 ℃, showing the formation of minor amounts of secondary $FeNi_3$ (#88-1715) phases at 2θ=44° and 51° for x=0–0.2. Fig. 1(b) also shows that diffraction peaks from $FeNi_3$ decreased with the La^{3+} dopant increasing, which became difficult to be detected at x=0.3 and 0.4. These results suggest that doping La^{3+} in the A-site seemingly inhibit the *in-situ* exsolution behavior of $Sr_2Fe_{1.5}Ni_{0.1}Mo_{0.4}O_{6-\delta}$ oxides and thereby enhance the structural stability of La_xSFNM oxides in the reducing environments.

To better understand the influence of lanthanum dopants on the exsolution behavior and the resulting morphology of nanoparticulates, a series of La_xSFNM (x=0, 0.1, 0.2, 0.3, 0.4) pellets were prepared at 1400 ℃ in air and then reduced in 10vol% H_2/N_2 at 750 ℃ for 4 h. Fig. 2 shows the surface morphologies of as-prepared and reduced perovskite oxides. The as-prepared SFNM sample shows clean and smooth grains without any visible secondary phases (Fig. 2(a)). Upon reduction, many nano-scale particles exsolved and homogeneously distributed on the oxide surface (Fig. 2(b-f)). EDS analysis confirms that these precipitated nanoparticulates exist largely as Fe-Ni alloys (Fig. 3), consistent with the XRD peaks of $FeNi_3$ in Fig.1(b). The diameter of Fe-Ni alloy nanoparticles is 40–60 nm. Fig. 2 also shows that the density of exsolved nanoparticulates on the oxide surface decreases significantly with the La^{3+} dopant increasing, supporting the conclusion from the XRD analysis that doping La^{3+} in the A-site helps to inhibit the exsolution of metal nanoparticulates and thus improve the structural stability of the pristine perovskite oxides.

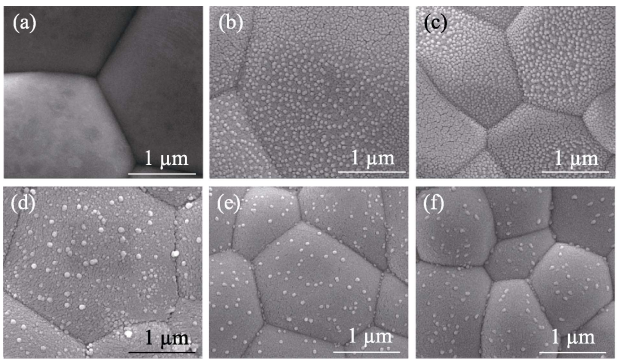

Fig. 2　Surface morphologies of (a) SFNM ceramic pellets before reduction and (b-f) La_xSFNM ceramic pellets after reduction in humidified 10vol% H_2/N_2 (3vol% H_2O) at 750 ℃ for 4 h
(b) SFNM; (c) $La_{0.1}SFNM$; (d) $La_{0.2}SFNM$; (e) $La_{0.3}SFNM$; (f) $La_{0.4}SFNM$

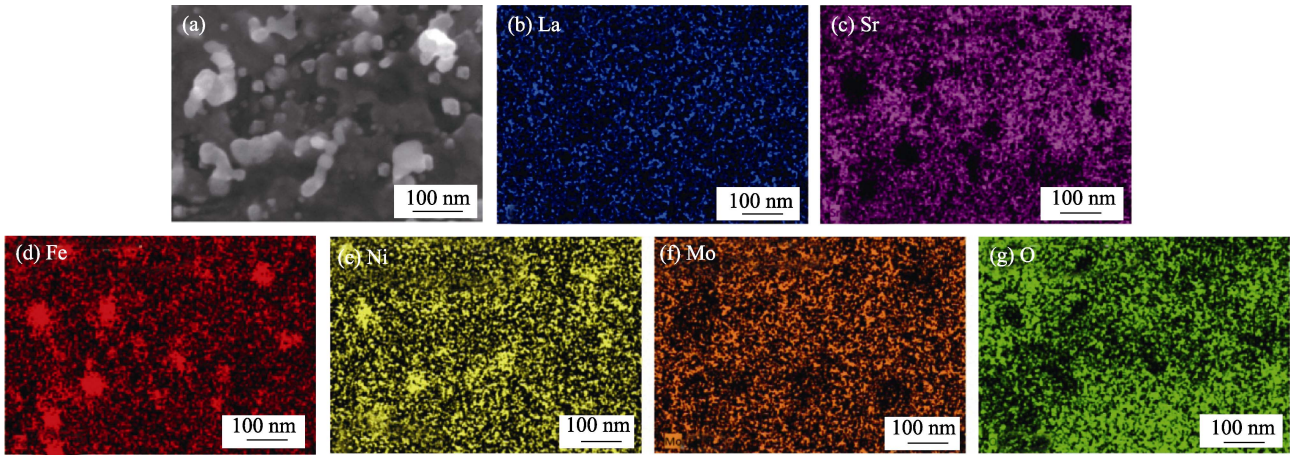

Fig. 3　(a) SEM image of reduced $La_{0.3}SFNM$ ceramic surface and (b-g) elemental mapping of La (b, blue), Sr (c, magenta), Fe (d, red), Ni (e, yellow), Mo (f, brown) and O (g, green)

The polarization resistance provides a quantitative measurement of the catalytic activity of La_xSFNM oxides toward electro-oxidation of hydrogen, which can be readily obtained from impedance measurements on symmetrical anode fuel cells, *i.e.*, Nano-La_xSFNM@LSGM|LSGM|Nano-La_xSFNM@ LSGM. Fig. 4(a) summarizes Nyquist plots of impedance spectra measured at 750 ℃ in a homogeneous environment of 97vol% H_2–3vol% H_2O for symmetrical anode fuel cells with varied La^{3+} dopants, where the ohmic resistances due to the electrolytes and the collecting wires were removed and the polarization resistances were divided by two to account for contributions of two symmetrical anodes. The anode specific polarization resistances ($R_{P,A}$) are taken as the overall widths of depressed arcs in Fig. 4(a). The anode polarization resistance is $R_{P,A}$=0.21 Ω·cm^2 for SFNM, decreases gradually with the La^{3+} dopant increasing, and attains a minimal value of 0.16 Ω·cm^2 at x=0.3. Further increasing the La^{3+} dopant yields a slightly increased $R_{P,A}$ value (0.17 Ω·cm^2) for $La_{0.4}$SFNM cell. The Bode plots of impedance data in Fig. 4(b) show that the response difference mainly occurs over the frequency range of 10–1000 Hz. Analysis of Distribution of Relaxation Time (DRT) was performed to effectively separate the multiple time constants[23-24], with the results summarized in Fig. 4(c). Notably, the impedance spetra consist of three different processes (denoted as R_H, R_M, R_L) in the frequency range of 100–1000, 10–100 and 0.1–10 Hz, respectively. Similar to the SFNM anode, the high-frequency resistance R_H relates to charge transfer across the electrolyte/electode interface, whereas the medium- and low-frequency resistances (R_M and R_L) are associated with the surface reactions[13,25]. Increasing the La^{3+} dopant yields a pronounced decrease in R_M with R_H and R_L almost unchanged, indicating that doping La^{3+} in the A-site effectively promotes the surface reaction on the perovskite oxides. Since the SEM observations show inhibited exsolution of $FeNi_3$ nanoparticulates and increased stability of the perovskite oxides with more La^{3+} dopants, the optimal catalytic activity at x=0.3 may be associated with the synergy between the exsolved catalysts and the supporting perovskite oxides.

The anode behavior was further examined on the functioning fuel cells as fabricated from tri-layer structures of "porous|dense|porous" LSGM. The dense LSGM electrolytes are typically ~22 μm thick (Fig. 5(a)). SBSCO and $La_{0.3}$SFNM were impregnated into the two porous LSGM scaffolds, respectively. High magnification view of the anode after the fuel cell measurements show the formation of *in situ* exsolved nanoparticulates on the surface of $La_{0.3}$SFNM oxides (Fig. 5(b)). Fig. 6(a) shows the representative polarization curves of the cell voltages (V) and power densities (P) as functions of current densities (J) for the single cells with $La_{0.3}Sr_{1.55}Fe_{1.5}Ni_{0.1}Mo_{0.4}O_{6-\delta}$ as anode catalyst. The maximum power densities are 1.26, 1.13, 0.90, 0.74 and 0.52 W·cm^{-2} at 750, 700, 650, 600 and 550 ℃, respectively. Cells with varied La^{3+} doped anodes were also prepared and measured under similar conditions, with the results compared in Fig. 6(b). The cells (x=0.3) exhibit the highest power densities at all temperatures. The present values are also much higher than previously reported power densities, *e.g.*, 0.59 W·cm^{-2} for SFNiM[13] and 0.85 W·cm^{-2} for SFM[26] at 750 ℃.

Long-term stability of nano-scale $FeNi_3$ catalysts as shown in Fig. 2 is very questionable due to their high susceptibility to continuous agglomeration and coarsening at elevated temperatures. Although extended measurements are required for better evaluation of the long-term stability of these nano-scale catalysts, some of the cells were operated for a few hundred hours. Fig. 7 shows a representative plot of the cell voltage as a function of time. The single cell was run at 0.5 A·cm^{-2} under 550 ℃ for 120 h, followed by another 80 h operation at 1.0 A·cm^{-2}, 650 ℃, showing negligible decay in the power output at both temperatures. These results demonstrate great promise of $La_{0.3}Sr_{1.55}Fe_{1.5}Mo_{0.4}Ni_{0.1}O_{6-\delta}$ as efficient catalyst for electro-oxidation of hydrogen fuels.

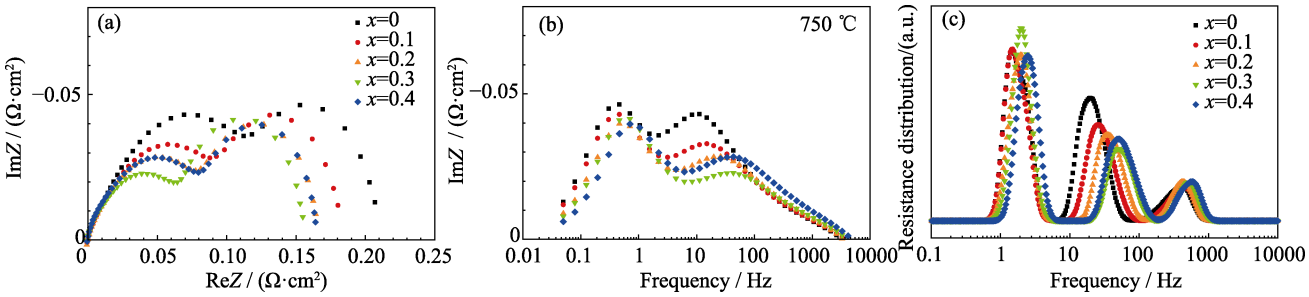

Fig. 4 (a) Nyquist and (b) Bode plots of impedance data for symmetrical anode fuel cells, *i.e.*, Nano-La_xSFNM@LSGM | LSGM | Nano-La_xSFNM@ LSGM, operating in humidified H_2 (3vol% H_2O, 100 mL·min^{-1}) at 750 ℃, (c) distributions of relation time (DRT) plots of the data shown in (a) and (b)

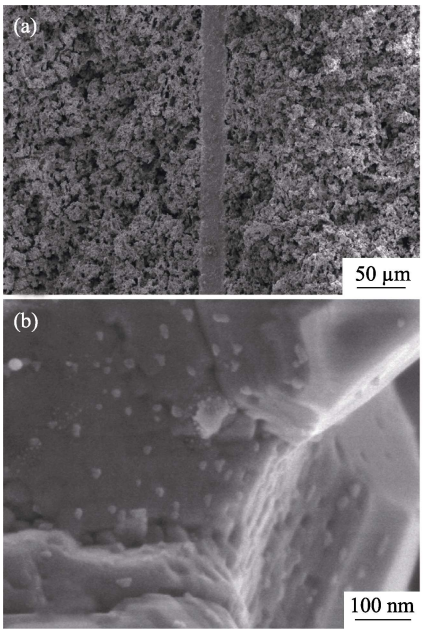

Fig. 5　(a) Cross-sectional micrograph of measured fuel cell (Nano-$La_{0.3}$SFNM@LSGM|LSGM|Nano-SBSCO@LSGM), and (b) high magnification view of the impregnated catalyst

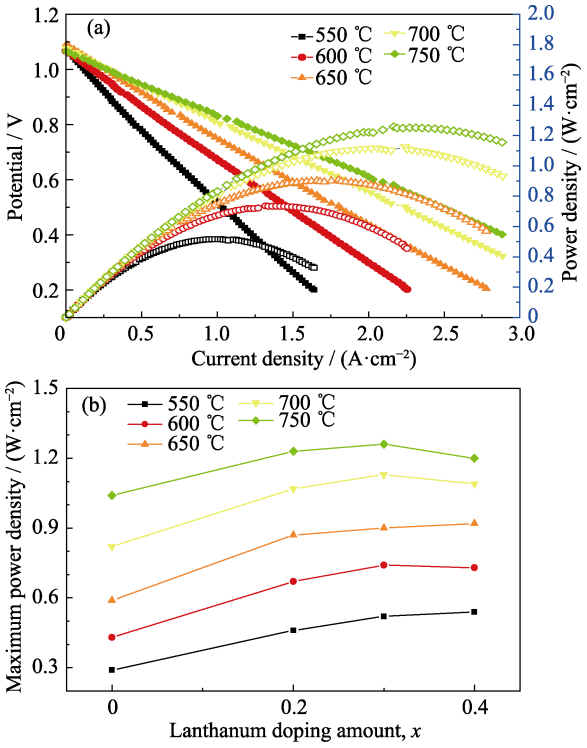

Fig. 6　(a) Voltage and power density *versus* current density for the functioning fuel cell (Nano-$La_{0.3}$SFNM@LSGM|LSGM|Nano-SBSCO@LSGM), measured in 97vol% H_2-3vol% H_2O at 100 sccm; (b) Peak power densities at different temperatures for single cells with varied La_xSFNM anodes

3　Conclusion

In summary, a series of $La_xSr_{2-3x/2}Fe_{1.5}Ni_{0.1}Mo_{0.4}O_{6-\delta}$ (x=0–0.4) oxides were synthesized, and their structural stability in reducing environments was examined. Both XRD patterns and SEM observations confirm the exsolution of nano-scale $FeNi_3$ particles on the oxide surface after the thermal treatment in H_2. Increasing the La^{3+} dopant enhances the structural stability of these oxides with inhibited exsolution of $FeNi_3$ nanoparticulates. Synergy between the exsolved $FeNi_3$ nanoparticulates and the supporting oxides yields the highest catalytic activities toward hydrogen oxidation reactions with the lowest polarization resistances at x=0.3, *e.g.*, 0.16 Ω·cm^2 at 750 ℃. Thin LSGM electrolyte SOFCs with nano-$La_{0.3}Sr_{1.55}Fe_{1.5}Mo_{0.4}Ni_{0.1}O_{6-\delta}$@LSGM anodes and nano-SBSCO@LSGM cathodes produces peak power densities of 1.26, 0.90 and 0.52 W·cm^{-2} at 750, 650 and 550 ℃, respectively.

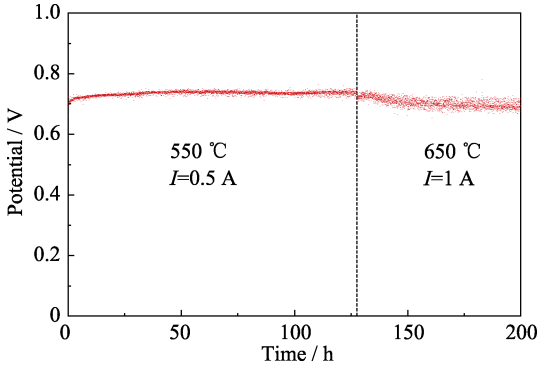

Fig. 7　Cell voltage as a function of operation time for the single fuel cell (Nano-$La_{0.3}$SFNM@LSGM|LSGM|Nano-SBSCO@LSGM), operated under constant current density at 550 and 650 ℃

References:

[1] CASSIDY M, LINDSAY G, KENDALL K. The reduction of nickel-zirconia cermet anodes and the effects on supported thin electrolytes. *Journal of Power Sources*, 1996, **61(1):** 189–192.

[2] SLATER R P, FAGG D P, IRVINE J T S. Synthesis and electrical characterization of doped perovskite titanates as potential anode materials for solid oxide fuel cells. *Journal of Materials Chemistry*, 1997, **7(12):** 2495–2498.

[3] TAO S, IRVINE J T S. A redox-stable efficient anode for solid-oxide fuel cells. *Nature Materials*, 2003, **2(5):** 320.

[4] LIU Q, DONG X, XIAO G, *et al.* A novel electrode material for symmetrical SOFCs. *Advanced Materials*, 2010, **22(48):** 5478–5482.

[5] DU Z H, ZHAO H L, LI S M, *et al.* Exceptionally high performance anode material based on lattice structure decorated double perovskite $Sr_2FeMo_{2/3}Mg_{1/3}O_{6-\delta}$ for solid oxide fuel cells. *Advanced Energy Materials*, 2018, **8(18):** 1800062.

[6] YANG G, FENG J, SUN W, *et al.* The characteristic of strontium-site deficient perovskites $Sr_xFe_{1.5}Mo_{0.5}O_{6-\delta}$($x$=1.9–2.0) as intermediate-temperature solid oxide fuel cell cathodes. *Journal of Power Sources*, 2014, **268:** 771–777.

[7] HE B, ZHAO L, SONG S, *et al.* $Sr_2Fe_{1.5}Mo_{0.5}O_{6-\delta}$-$Sm_{0.2}Ce_{0.8}O_{1.9}$ composite anodes for intermediate-temperature solid oxide fuel cells. *Journal of The Electrochemical Society*, 2012, **159(5):** B619–B626.

[8] XIAO G L, CHEN F L. Ni modified ceramic anodes for direct-methane solid oxide fuel cells. *Electrochemistry Communications*, 2011, **13(1):** 57–59.
[9] XIAO G L, JIN C, LIU Q, *et al.* Ni modified ceramic anodes for solid oxide fuel cells. *Journal of Power Sources*, 2012, **201:** 43–48.
[10] LIU Z, LIU B, DING D, *et al.* Fabrication and modification of solid oxide fuel cell anodes *via* wet impregnation/infiltration technique. *Journal of Power Sources*, 2013, **237:** 243–259.
[11] TSEKOURAS G, NEAGU D, IRVINE J T S. Step-change in high temperature steam electrolysis performance of perovskite oxide cathodes with exsolution of B-site dopants. *Energy Environ. Sci*., 2012, **6(1):** 256–266.
[12] NEAGU D, TSEKOURAS G, MILLER D N, *et al. In situ* growth of nanoparticles through control of non-stoichiometry. *Nature Chemistry*, 2013, **5(11):** 916–923.
[13] DU Z, ZHAO H, YI S, *et al.* High-performance anode material $Sr_2FeMo_{0.65}Ni_{0.35}O_{6-\delta}$ with *in situ* exsolved nanoparticle catalyst. *ACS Nano*, 2016, **10(9):** 8660–8669.
[14] GAO Y, WANG J, LYU Y Q, *et al. In situ* growth of Pt_3Ni nanoparticles on an A-site deficient perovskite with enhanced activity for the oxygen reduction reaction. *J. Mater. Chem. A*, 2017, **5(14):** 6399–6404.
[15] MAHATO N, BANERJEE A, GUPTA A, *et al.* Progress in material selection for solid oxide fuel cell technology: a review. *Prog. Mater. Sci*., 2015, **72:** 141–337.
[16] WANG Y, LIU T, LI M, *et al.* Exsolved Fe–Ni nano-particles from $Sr_2Fe_{1.3}Ni_{0.2}Mo_{0.5}O_6$ perovskite oxide as a cathode for solid oxide steam electrolysis cells. *Journal of Materials Chemistry A*, 2016, **4(37):** 14163–14169.
[17] ZHU T, TROIANI H E, MOGNI L V, *et al.* Ni-substituted $Sr(Ti,Fe)O_3$ SOFC anodes: achieving high performance *via* metal alloy nanoparticle exsolution. *Joule*, 2018, **2(3):** 478–496.
[18] MYUNG J, NEAGU D, MILLER D N, *et al.* Switching on electrocatalytic activity in solid oxide cells. *Nature*, 2016, **537(7621):** 528–531.
[19] LEE W, HAN J W, CHEN Y, *et al.* Cation size mismatch and charge interactions drive dopant segregation at the surfaces of manganite perovskites. *J. Am. Chem. Soc*., 2013, **135 (21):** 7909–7925.
[20] GÁLVEZ M E, JACOT R, SCHEFFE J, *et al.* Physico-chemical changes in Ca, Sr and Al-doped La–Mn–O perovskites upon thermochemical splitting of CO_2 *via* redox cycling. *Physical Chemistry Chemical Physics*, 2015, **17(9):** 6629–6634.
[21] MUÑOZ-GARCÍA A B, BUGARIS D E, PAVONE M, *et al.* Unveiling structure–property relationships in $Sr_2Fe_{1.5}Mo_{0.5}O_{6-\delta}$, an electrode material for symmetric solid oxide fuel cells. *Journal of the American Chemical Society*, 2012, **134(15):** 6826–6833.
[22] MENG X, HAN D, WU H, *et al.* Characterization of $SrFe_{0.75}Mo_{0.25}O_{3-\delta}$–$La_{0.9}Sr_{0.1}Ga_{0.8}Mg_{0.2}O_{3-\delta}$ composite cathodes prepared by infiltration. *Journal of Power Sources*, 2014, **246:** 906–911.
[23] XIAO G, LIU Q, ZHAO F, *et al.* $Sr_2Fe_{1.5}Mo_{0.5}O_6$ as cathodes for intermediate-temperature solid oxide fuel cells with $La_{0.8}Sr_{0.2}Ga_{0.87}Mg_{0.13}O_3$ electrolyte. *J. Electrochem. Soc*., 2011, **158(5):** B455–B460.
[24] SACCOCCIO M, WAN T H, CHEN C, *et al.* Optimal regularization in distribution of relaxation times applied to electrochemical impedance spectroscopy: ridge and Lasso regression methods - a theoretical and experimental study. *Electrochimica Acta*, 2014, **147:** 470–482.
[25] DU Z H, ZHAO H L, YANG C Y, *et al.* Optimization of strontium molybdate based composite anode for solid oxide fuel cells. *J. Power Sources*, 2015, **274:** 568–574.
[26] MENG X, LIU X J, HAN D, *et al.* Symmetrical solid oxide fuel cells with impregnated $SrFe_{0.75}Mo_{0.25}O_{3-\delta}$ electrodes. *J. Power Sources*, 2014, **252:** 58–63.

固体氧化物燃料电池 $La_xSr_{2-3x/2}Fe_{1.5}Ni_{0.1}Mo_{0.4}O_{6-\delta}$ 阳极性能研究

夏 天[1,2], 孟 燮[1], 骆 婷[1], 占忠亮[1]

(1. 中国科学院 上海硅酸盐研究所, 能量转换材料重点实验室, 上海 200050; 2. 中国科学院大学, 北京 100049)

摘 要: 本研究利用固相反应法合成了一系列镧取代 $La_xSr_{2-3x/2}Fe_{1.5}Ni_{0.1}Mo_{0.4}O_{6-\delta}$ (La_xSFNM, x=0, 0.1, 0.2, 0.3, 0.4)钙钛矿陶瓷材料, 并研究其作为固体氧化物燃料电池阳极的电化学性能。X 射线衍射(XRD)测试表明合成的粉末具有立方钙钛矿结构。在高温下利用氢气还原 La_xSFNM 样品, 发现其晶粒表面析出纳米尺度的 Fe-Ni 合金颗粒, 并且偏析纳米颗粒的密度随着 La^{3+}掺杂量的增加而显著降低。在对称电池阻抗测试中, 随着 La^{3+}掺杂量的增加, 阳极极化阻抗逐渐降低, 掺入量为 0.3 时阻抗达到最小值。$La_{0.3}$SFNM 对称电池在 750 ℃下极化阻抗仅为 0.16 Ω·cm^2, 进一步增加掺杂量时, $La_{0.4}$SFNM 对称电池极化阻抗增加至 0.17 Ω·cm^2。$La_{0.3}$SFNM 材料良好的电极反应催化活性源于适当分布的 Fe-Ni 合金纳米偏析颗粒与 La_xSFNM 陶瓷基体的共同作用。利用流延法制备一系列以 La_xSFNM 为阳极、$SmBa_{0.5}Sr_{0.5}Co_2O_6$ 为阴极、LSGM 为电解质的单电池, 使用氢气作为燃料时, La^{3+}掺杂量 x=0.3 的单电池表现出最高的功率密度, 在 750、650 和 550 ℃时峰值功率密度可达 1.26、0.90 和 0.52 W·cm^{-2}。上述结果表明, $La_{0.3}Sr_{1.55}Fe_{1.5}Ni_{0.1}Mo_{0.4}O_{6-\delta}$ 可以用作高性能 SOFC 阳极催化剂。

关 键 词: 固体氧化物燃料电池; 阳极材料; 高温原位脱溶

中图分类号: TM911 **文献标识码:** A